Optical and Piezoelectric Properties of Strained Orthorhombic PdS_2

Shuo Deng, Menglun Tao, Jie Mei, Min Li, Yan Zhang and Lijie Li, *Senior Member, IEEE*

***Abstract*— We investigate optical and piezoelectric properties of the orthorhombic PdS_2 under symmetrical biaxial tensile strains with various magnitudes. The *ab initio* simulation results found that the peaks of the refractive index, extinction coefficient, absorption coefficient and reflectivity of the orthorhombic PdS_2 red-shift with the tensile strains. Specifically, we discover that the absorption coefficient of the strained orthorhombic PdS_2 (4.01×10^5 /cm - 5.52×10^5 /cm) is much higher than traditional optoelectronics, piezoelectric and piezophototronic materials such as Si, Ge, GaInAs, ZnO and monolayer MoS_2 demonstrating much wider absorption spectrum (670 nm - 1033 nm). Moreover, the piezoelectric constant of the orthorhombic PdS_2 is calculated from 0 to 8% tensile strains. Simulation results show the orthorhombic PdS_2 with 4% tensile strain has a strong piezoelectric effect (1.33 C/m^2), which is 100-5000 times higher than other deformation magnitudes. The results indicate that the orthorhombic PdS_2 will have potential application in piezophotonic and piezoelectric devices.**

***Index Terms*— Optical property, piezoelectric property, PdS2, mechanical strain.**

I. Introduction

THE transition-metal dichalcogenides (TMDs) semiconductors have attracted considerable attention because their superior properties, such as an excellent electronic and optical tunability [1] [2], strong piezophotonic [3, 4] and piezoelectric effects [4, 5]. These excellent properties have resulted in many applications, such as phototransistor [6, 7], flexible optoelectronics [8], self-powered nanosystems [9, 10] and smart MEMS/NEMS [8, 11, 12]. During the last decade, several TMDs have been extensively investigated, both in theory and experiment [2, 13-17].

Previously, it was theoretically and experimentally demonstrated that some noble metals can form layered structures with four S atoms, like PdS_2 [18, 19]. Furthermore, some important properties distinguished from the traditional two-dimensional (2D) TMDs have been reported , such as excellent linear electronic and optical tunability [2]. Many previous studies have shown that one can tune the electronic and optical properties of the TMDs by applying mechanical strains [2, 16, 17, 20-22]. Although the optical properties of the monolayer PdS_2, electron transport properties and stability of the bilayer and bulk PdS_2 have been studied in references[2, 23, 24], there are very few studies on the first principles analysis of the orthorhombic PdS_2. It is a need of analysis for the optical and piezoelectric properties of the orthorhombic PdS_2 under strains with different magnitudes.

In this work, we analysis the optical and piezoelectric properties of the orthorhombic PdS_2 under symmetrical biaxial tensile deformation ranging between 0 and 8% using the *ab initio* simulation and modern theory of polarization. These methods has been used in many previous studies on the TMDs and piezotronics [2, 16, 17, 22, 25-27]. Our aim is to theoretically explore the development of optical and piezoelectric properties for the orthorhombic PdS_2 under different tensile strains. Particularly, we focus on unveiling the possibility and prospects of deploying the orthorhombic PdS_2 in future tunable nano-electromechanical devices and smart sensors.

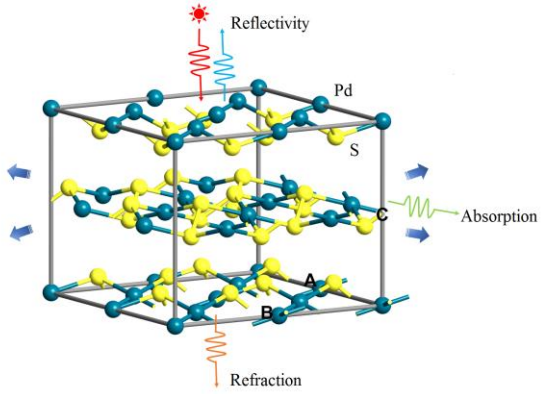

Fig. 1. Schematic graph for strain modulation of the orthorhombic PdS_2

II. Computational Method

In this work, we investigate strain-dependent optical and

Manuscript accepted March 26 2019.

This work was supported by the China Scholarship Council (CSC). S. Deng, Menglun Tao and Jie Mei are with the School of Logistic Engineering, Wuhan University of Technology, Wuhan, 430070, China. Min Li is with the Department of Physics, Wuhan University of Technology, Wuhan, 430070, China. Yan Zhang is with the School of Physics, University of Electronic Science and Technology, Chengdu 610054, China. Lijie Li is with the Systems and Process Engineering Centre, College of Engineering, Swansea University, Swansea, SA1 8EN, UK. (Corresponding author: Lijie Li, e-mail: L.Li@swansea.ac.uk)

piezoelectric properties of the orthorhombic PdS_2 by using the density functional theory (DFT) based on the Atomistix ToolKit (ATK)[28]. As seen in Fig. 1, the orthorhombic structure is composed of 2D S-Pd-S layers stacking along the *c* axis which are well separated from each other with apparently van der Waals gaps. We started from the key lattice constants of the orthorhombic structure with *a*=5.502 Å, *b*=5.594 Å and *c*=8.607 Å[29]. The Hermann-Mauguin, hall, point group and crystal system of the optimized structure are Pbca, -P 2ac 2ab, mmm and orthorhombic, respectively. In the practical simulation, the exchange correlation potentials use the generalized gradient approximation (GGA) with the parametrization of Perdew-Burke–Ernzerhof (PBE)[30] and the mesh cut-off energy of 75 Hartree with 10×10×10 k-points. The Limited-memory Broyden Fletcher Goldfarb Shanno (LBFGS) algorithm with the maximum stress tolerance value of 0.01 eV/Å^3 is used. The band gap of the orthorhombic PdS_2 is calculated using the Meta-GGA (MGGA.TB09LDA), which not only include the local density and the gradient of the density approximation, but also the kinetic energy density approximation[31, 32]. Note that the symmetrical biaxial tensile strains along the A (ε_a) and B (ε_b) direction within the plane are shown in Fig. l. The deformation is simulated by setting the lattice parameter to a fixed larger value and relaxing the atomic positions. The magnitude of strain is defined as $\Delta\varepsilon = (a - a_0)/a_0$, where a_0 and a are the equilibrium and strained lattice values, respectively. The crystal structure of the PdS_2 is similar to that of graphite, which consists of multiple 2D layers bonded by van der Waals (vdW) forces. In our model, we set the *x/y* plane as the 2D layer plane, therefore the vdW interactions only exist in *z*- direction. In our original model, we considered the interlayer vdW interactions in the geometry optimization of bulk PdS_2, we used the semi-empirical corrections by Grimme DFT-D2 model, which takes account the long-range vdW interaction [33]. When we apply symmetrical biaxial tensile strains along the A (ε_a) and B (ε_b) direction within the *x/y* plane, the strain effect of bulk PdS_2 only appears in the *x/y* plane, and there is no strain in *z*- direction.

III. Optical Property

We calculated the optical property of the orthorhombic PdS_2 under the tensile strains. By the Kubo-Greenwood formula, the susceptibility tensor at a frequency ω has the form as[34].

$$\chi_{ij}(\omega) = -\frac{e^2\hbar^4}{m^2\epsilon_0 V\omega^2}\sum_{nm}\frac{f(E_m)-f(E_n)}{E_{nm}-\hbar\omega-i\Gamma}\pi^i_{nm}\pi^j_{mn} \quad (1)$$

where e, $\hbar$ and ϵ_0 are the elementary charge, reduced Planck constant and vacuum dielectric constant respectively. π^i_{nm} is the *i*-th component of the dipole matrix element between state *n* and *m*. E_m, E_n and E_{nm} are the energy level at *m*, *n* and energy difference between the state *n* and *m*. *V*, Γ and *f* are the volume, broadening and Fermi function, respectively. The relative dielectric constant (ϵ_r) are related to the susceptibility as:

$$\epsilon_r(\omega) = (1 + \chi(\omega)) \quad (2)$$

The complex dielectric constant can be expressed as:

$$\epsilon(\omega) = \epsilon_0\epsilon_r(\omega) = \epsilon_1(\omega) + \epsilon_2(\omega) \quad (3)$$

where, ϵ_0, ϵ_1 and ϵ_2 are the vacuum dielectric constant, real and imaginary parts of the complex dielectric constant, respectively.

The real and imaginary parts of the complex dielectric constant can be calculated from the Kramers-Kronig relations:

$$\epsilon_1(\omega) = 1 + \frac{2}{\pi}A\int_0^\infty \frac{\omega'\epsilon_2(\omega')}{\omega^{2\prime}-\omega^2}d\omega' \quad (4)$$

$$\epsilon_2(\omega) = -\frac{2\omega}{\pi}A\int_0^\infty \frac{\epsilon_1(\omega')}{\omega^{2\prime}-\omega^2}d\omega' + \frac{\sigma_0}{\epsilon_0\omega} \quad (5)$$

where, A and σ_0 are the principal part of the integral and DC conductivity. The refractive index (n) and extinction coefficient (κ) are related to the complex dielectric constant through $n + i\kappa = \sqrt{\epsilon(\omega)}$. In terms of the real and imaginary parts of the complex dielectric constant, the refractive index and extinction coefficient are given by:

$$n = \sqrt{\frac{\sqrt{\epsilon_1^2+\epsilon_2^2}+\epsilon_1}{2}} \quad (6)$$

$$\kappa = \sqrt{\frac{\sqrt{\epsilon_1^2+\epsilon_2^2}-\epsilon_1}{2}} \quad (7)$$

The optical absorption coefficient (α_a) is related to the extinction coefficient through:

$$\alpha_a = 2\frac{\omega}{c}\kappa \quad (8)$$

where, ω and *c* are the angular frequency and the speed of light. The reflectivity (*r*) is given by:

$$r = \frac{(1-n)^2+\kappa^2}{(1+n)^2+\kappa^2} \quad (9)$$

The real and imaginary parts of the complex dielectric constant for biaxial tensile strains on the orthorhombic PdS_2 are calculated, and results are shown in Fig. 2. Here, we only calculated the deformation with strains at *a* and *b* ranging from 0 to 8%, since larger deformation values can potentially induce instability and are very difficult to achieve in experiment. We calculated the stress-strain relation of the bulk PdS_2 in the tensile strain range of 0 - 14% in Fig. 3. As the applied tensile strain increases ($|\Delta\varepsilon| > 8\%$), the calculated stress-strain behaviours become nonlinear. Under large deformations, mechanical nonlinearity causes significant change of geometry structure [35]. Based on the calculated stress-strain curve, it appears that the bulk PdS_2 is relatively stable from 0 to 8% tensile strains. The peak wavelength of the real part (ϵ_1) shifts from around 750 nm to 1550 nm, while the peak wavelength of the imaginary part (ϵ_2) shifts from around 690 nm to 1080 nm under the tensile deformation varying from 0 to 8%. For the

largest strain, the amplitudes of both the real and imaginary parts are much higher, which demonstrates that a large number of inter-band transitions occur at this energy, corresponding to the concentrated band near the Fermi level. Moreover, it is clear from Fig. 2 that the peak wavelengths of the real and imaginary

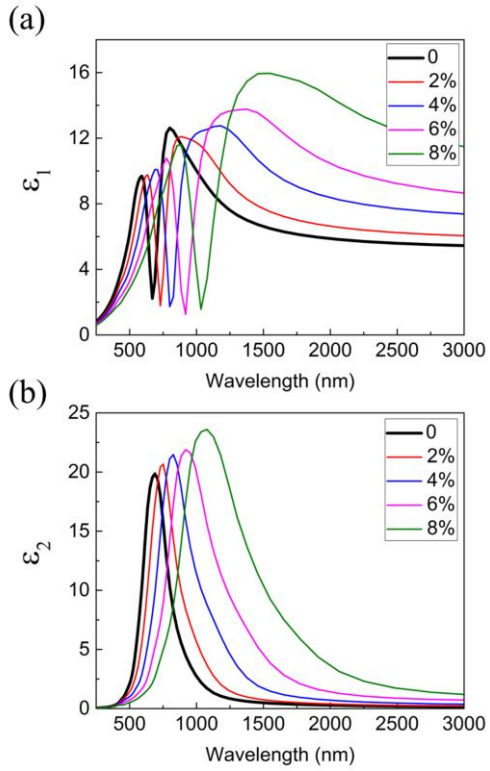

Fig. 2. The real (a) and imaginary (b) parts of the complex dielectric constant spectrums of the orthorhombic PdS_2 along biaxial tensile strains.

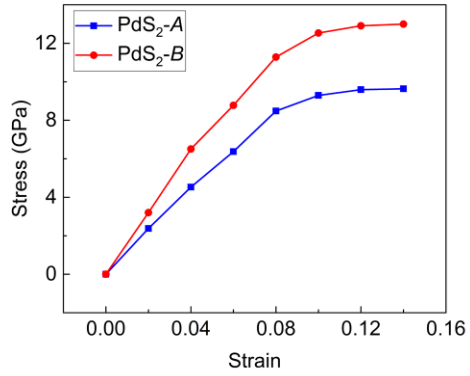

Fig. 3. Stress-strain relation of the bulk PdS_2 from 0 to 14% tensile strains under the *a* and *b* direction.

dielectric constant can be red-shifted when the strain varies from 0 to 8%.

Fig. 4 shows the simulated refractive index, extinction coefficient, reflectivity and absorption coefficient spectrums relating to the wavelength for biaxial tensile strains on the orthorhombic PdS_2. The bold black lines in Fig. 4 are the spectrums without strain. The first observation reveals that the peak wavelengths of the refractive index, extinction coefficient, reflectivity and absorption coefficient shift toward longer wavelengths. This red-shift is almost uniform with the increasing strain value. Second, the peak amplitudes of the refractive index, extinction coefficient and reflectivity increase with the increase of the tensile deformation. However, the change of the absorption coefficient is the opposite to the refractive index, extinction coefficient and reflectivity. Third, it is clear from Fig. 4(a) that the refractive index has two different peaks under the same tensile deformation and the gap of the two peaks increases with the tensile strains.

Fig. 5 shows the refractive index, reflectivity and absorption coefficient of the orthorhombic PdS_2 compared with the theoretical prediction values of traditional optoelectronic, piezoelectric and piezophototronic materials (Si, Ge, GaInAs, ZnO and monolayer MoS_2) at various wavelengths. The electrical conductivity of Si, Ge, GaInAs, ZnO and orthorhombic PdS_2 are 10 S/cm[36], 20 S/cm[36], 12.8 S/cm[37], 0.61 S/cm[38] and 0.01 S/cm[39], respectively. The refractive index of the orthorhombic PdS_2 is slightly different from other three optoelectronic materials at the same wavelength. In Fig. 5, the reflectivity of the orthorhombic PdS_2 is 1.5-10 times higher than other optoelectronic materials. Results on the absorption coefficient shows that the orthorhombic PdS_2 demonstrates much higher values, especially in the strained states (shown in Fig. 3(d)). Compared with the Si, Ge, GaInAs, ZnO and monolayer MoS_2, the absorption coefficient of the orthorhombic PdS_2 is much higher, i.e. more than 2-3 orders of magnitude than the ZnO and 1-2 orders of magnitude than the monolayer MoS_2. Detailed comparison is made in Fig. 5. It indicates that the orthorhombic PdS_2 could potentially be used for enhancing the efficiency in piezophototronic devices and improving the sensitivity of the optical sensors.

To understand the origin of the strain induced red-shift for the above optical characteristics, we take a closer look at the strain-dependent band structures and partial density of states (PDOS) for various strain values. We calculated band structures of the Brillouin zone of high symmetry points for biaxial tensile strains on the orthorhombic PdS_2 under the strain varying from 0 to 8%, as shown in Fig. 6(a). The bands when zero strain is applied are marked by the bold black lines and the bands with different colors denote the bands under different deformations. Under the zero strain, the orthorhombic PdS_2 is an indirect band gap semiconductor with the conduction band minimum (CBM) and valence band maximum (VBM) at the *Y*-*S* and *G* point, respectively. Upon increasing the tensile strain, the CBM decreases and VBM increases. Both the CBM and VBM are maintained at the *Y*-*S* and *G* point. Fig. 4(b) shows the evolution of the CBM, VBM and band gap with the biaxial tensile strains. The common feature in Fig. 6(b) is that all curves are linear. The CBM and band gap linearly decrease, while the VBM linearly increases. CBM and band gap have the maximum values at the strain-free state, and minimum values at the maximum strain applied, while VBM has the reverse trend. This is similar with previous reported results about the monolayer

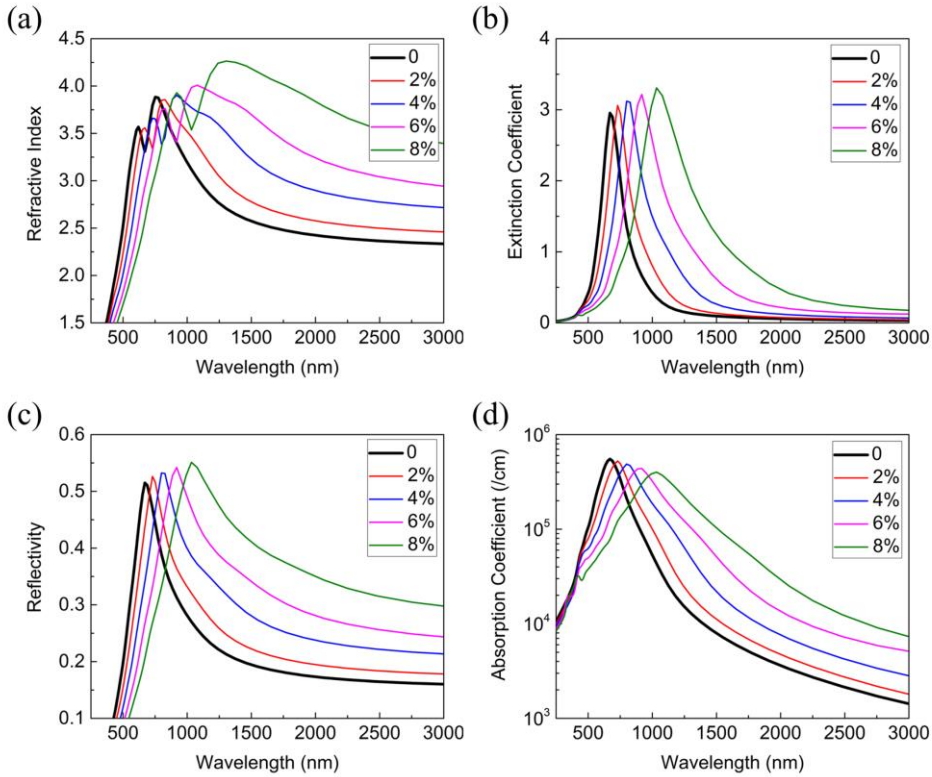

Fig. 4. The refractive index (a), extinction coefficient (b), reflectivity (c) and absorption coefficient (d) spectrums of the orthorhombic PdS_2 along the biaxial tensile strains.

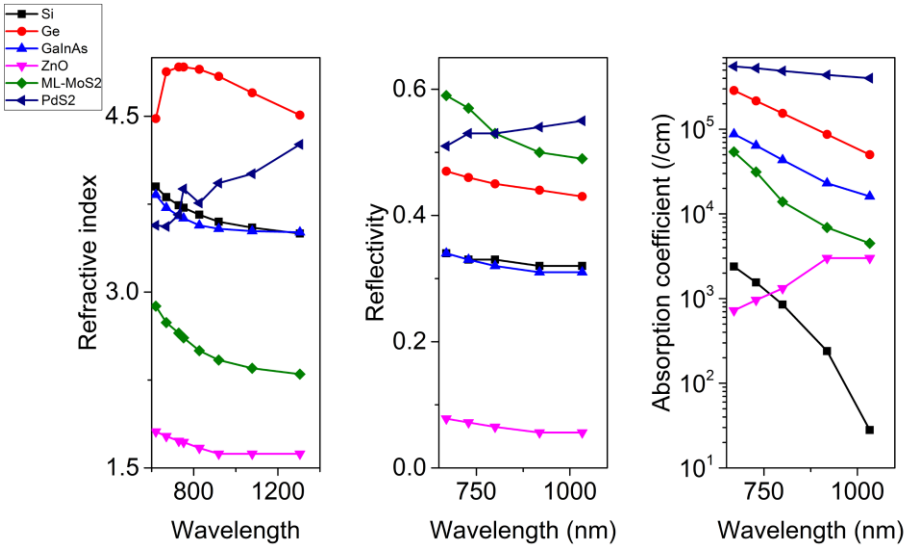

Fig. 5. Refractive index, reflectivity and absorption coefficient of Si, Ge, GaInAs, ZnO, monolayer MoS2 and orthorhombic PdS_2.

PdS_2 [2, 40, 41]. With the decrease of the band gap of the orthorhombic PdS_2, the peak wavelengths of the real and imaginary parts of the complex dielectric constants increase (red-shifted). This result is matching with the spectrums variation in Fig. 2.

Tensile strains on the orthorhombic PdS_2 alter bond lengths. Together with the confinement effects, optical properties are modified. To gain more physical insights on the change of optical properties of the orthorhombic PdS_2, Fig. 7 shows the partial density of states (PDOS) between -2 eV and 2 eV in the orthorhombic PdS_2 resolved into S-*s*, S-*p* and Pd-*d* orbital. In Fig. 7, the VBM and CBM are composed primarily of the S-*p* orbital and Pd-*d* orbital. The band gap and its size are determined by the manifold splitting due to the crystal field of the trigonal prismatic structure. As shown in Fig. 7, application of tensile strains decreases the coupling of the S-*p* orbital and Pd-*d* orbital, especially near the CBM, which is likely induced by the decrease of the bond length between the two S atoms and increase the bond length between the Pd and S atoms. Moreover, the VBM crosses the 0 eV under the 8% tensile deformation, which shows a strong capability of electrical transmission. Thus, we also calculated the transmission

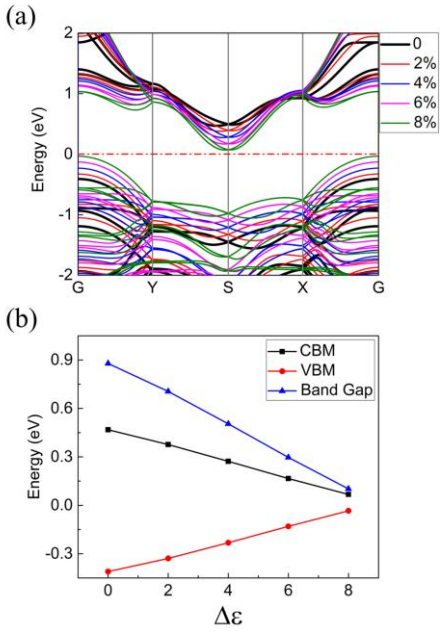

Fig. 6. The band structures of the orthorhombic PdS_2 with biaxial tensile strains (a) and the development of the CBM, VBM and band gap (b).

the *G* point (VBM), where k_A=k_B=0. Hence, the red-shift of the spectrums in the orthorhombic PdS_2 can be explained by the strain modulation of orbitals coupling and electrical transmission.

IV. Piezoelectric Property

In this section, we study the piezoelectric constant of the orthorhombic PdS_2. In the ATK software, the total macroscopic polarization P_{tm} of a solid is the sum of the spontaneous polarization P_{eq} and piezoelectric polarization P_p, which are the strain independent and strain dependent, respectively [42]:

$$P_{tm} = P_{eq} + P_p \tag{10}$$

The piezoelectric tensor (γ) can be expressed as:

$$\gamma = \frac{\Delta P_{tm}}{\Delta \varepsilon} \tag{11}$$

In our calculation, P_{tm} is calculated using the Berry-phase approach, which is evaluated using modern theory of polarization[42]. It is common to divide the polarization of the

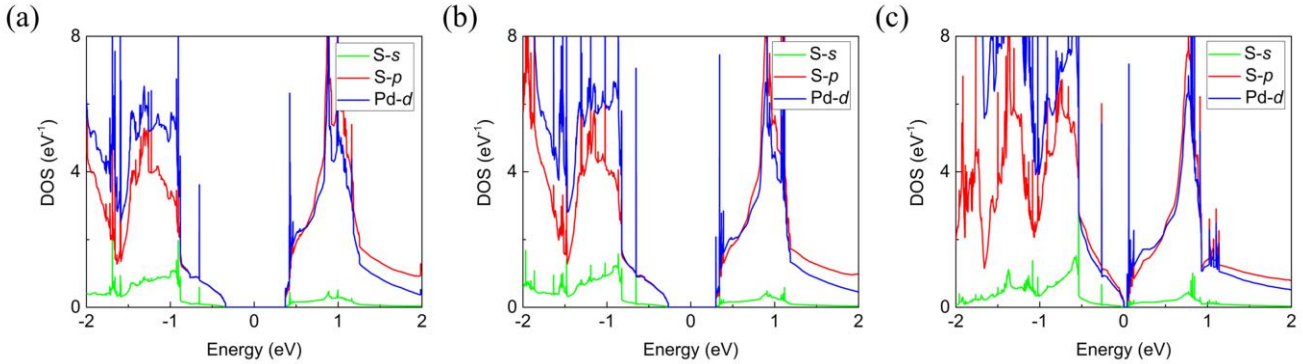

Fig. 7. The PDOS of the orthorhombic PdS_2 under the 0 (a), 4% (b) and 8% (c) biaxial tensile strain.

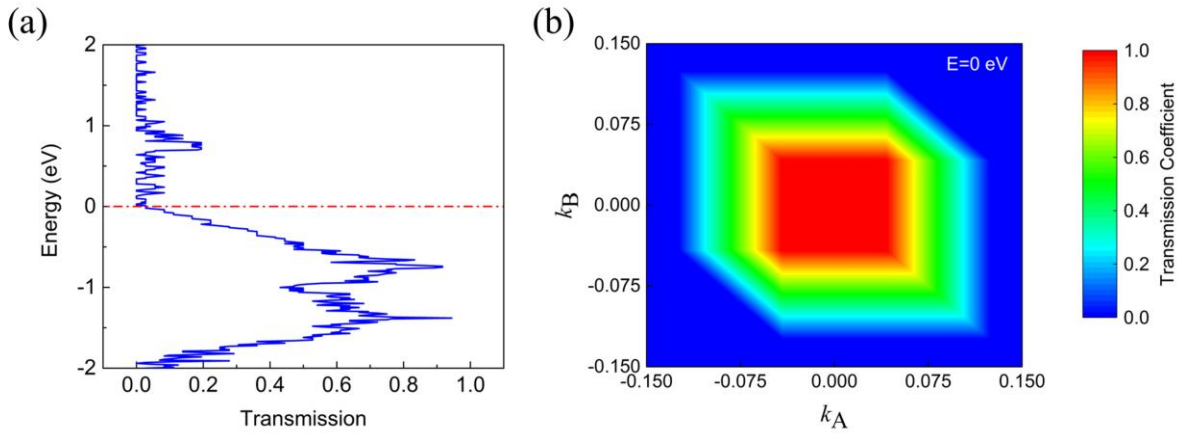

Fig. 8. The transmission spectrum (a) and average transmission coefficient at the 0 eV (b) under the 8% tensile deformation.

spectrum and average transmission coefficient at the 0 eV under the 8% tensile deformation in Fig. 8. it is clear that the main contributions to electrical transmission at the 0 eV come from the center of the Brillouin zone, which is the k-points around

materials into electronic and ionic parts. The total polarization ($\mathbf{P}_t$) is the sum of the electronic ($\mathbf{P}_i$) and ionic ($\mathbf{P}_e$) contributions:

$$\mathbf{P}_t = \mathbf{P}_i + \mathbf{P}_e \tag{12}$$

TABLE I
THE PIEZOELECTRIC CONSTANT, CLAMPED-ION TERM OF THE PIEZOELECTRIC CONSTANT, ELECTRONIC POLARIZATION, IONIC POLARIZATION AND TOTAL POLARIZATION OF THE ORTHORHOMBIC PdS_2

Deformation	e_{33} (C/m^2)	$e_{33}(0)$ (C/m^2)	$\mathbf{P}_i$	$\mathbf{P}_e$	$\mathbf{P}_t'$ (C/m^2)
0	-2.55×10^{-4}	-5.19×10^{-4}	-1.58×10^{-2}	1.43×10^{-2}	-3.94×10^{-4}
2%	3.90×10^{-4}	5.29×10^{-4}	-2.99×10^{-3}	4.72×10^{-3}	4.16×10^{-4}
4%	1.33×10^{0}	3.61×10^{-1}	-3.91×10^{-1}	3.39×10^{-1}	-1.40×10^{-2}
6%	-1.68×10^{-2}	-1.22×10^{-2}	4.57×10^{-1}	-4.86×10^{-1}	-7.78×10^{-3}
8%	-1.37×10^{-2}	1.30×10^{-2}	2.65×10^{-1}	-2.37×10^{-1}	7.58×10^{-3}

TABLE II
THE PIEZOELECTRIC CONSTANT, CLAMPED-ION TERM OF THE PIEZOELECTRIC CONSTANT FOR ORTHORHOMBIC PDS2 (4% TENSILE DEFORMATION), ZNO, GAN AND ALN.[43]

Material	e_{33} (C/m^2)	$e_{33}(0)$ (C/m^2)
PdS_2	1.33	0.36
ZnO	0.89	-0.66
GaN	0.73	-0.84
AlN	1.46	-0.47

As discussed in modern theory of polarization, all fractional polarizations are wrapped to the interval [-0.5, 0.5].

The electronic and ionic polarization parts can be calculated from:

$$\mathbf{P}_i = \frac{|e|}{\Omega}\sum_v Z_{ion}^v r^v \tag{13}$$

$$\mathbf{P}_e = -\frac{2|e|i}{(2\pi)^3}\int d\mathbf{k}_\perp \sum_{n=1}^{M}\int_0^{G_\parallel}\langle u_{\mathbf{k},n}|\frac{\partial}{\partial k_\parallel}|u_{\mathbf{k},n}\rangle\, dk_\parallel \tag{14}$$

where Z_{ion}^v and r^v are the valence charge and position vector of atom, Ω is the unit cell volume, $k_\parallel$ is parallel to the direction of polarization and $G_\parallel$ is a reciprocal lattice vector in the same direction. The states $|u_{\mathbf{k},n}>$ are the cell-periodic parts of the Bloch functions. This method computed the piezoelectric tensor of AlN bulk about 1.48 C/m^2, this value is in good agreement with the value found in the literature (1.46 C/m^2) [43], which verify the reliability of ATK software.

Table I summarizes the calculated piezoelectric constant (e_{33}), clamped-ion term of piezoelectric constant ($e_{33}(0)$), electronic polarization, ionic polarization and total polarization in Cartesian coordinates ($\mathbf{P}_t'$) of the orthorhombic PdS_2 under the tensile deformation varying from 0 to 8%. The calculation has confirmed that the orthorhombic PdS_2 with 4% tensile strain has a strong piezoelectric effect (1.33 C/m^2), which is higher than 2-3 orders of magnitude for other deformation values. Because of the sensitive dependence of the piezoelectric effects on the polarization, the total polarization under 4% tensile strain is -1.40×10^{-2} C/m^2 which is higher than other strain values. Moreover, the ionic polarization contributed primarily to the piezoelectric effect of the orthorhombic PdS_2 at 4% tensile strain. The ionic polarization occurs due to relative displacements between positive and negative ions in crystal. The 4% tensile strain induce relative displacements of the Pd and S atoms, the centers of positive and negative charges are also displaced. The locations of these centers are affected by the symmetry of the displacements, when the center doesn't correspond, polarizations arise in crystal. To facilitate further comparisons with other piezoelectric materials, in Table II we collect the experimentally measured values of piezoelectric constants for some traditional piezoelectric materials, such as ZnO, GaN and AlN [43]. The piezoelectric constant of the orthorhombic PdS_2 at 4% tensile strain is slightly less than AlN, while higher than ZnO and GaN. This result indicates that the orthorhombic PdS_2 could potentially be used for enhancing the efficiency in piezoelectric devices and increasing the sensitivity in strain sensors.

V. CONCLUSION

To summarize, *ab initio* simulation has been used to investigate the optical and piezoelectric properties of the orthorhombic PdS_2 under mechanical tensile strains. The orthorhombic PdS_2 has been modelled and subsequently simulated when subjecting to tensile strains. Main conclusions are drawn that the tensile strains introduce red-shift of the refractive index, extinction coefficient, absorption index and reflectivity. In addition, we found that the absorption coefficient of the strained orthorhombic PdS_2 (4.01×10^5 /cm - 5.52×10^5 /cm) is much higher than traditional optoelectronics, piezoelectric and piezophototronic materials (Si, Ge, GaInAs, ZnO and monolayer MoS_2), demonstrating much wider absorption spectrum (670 nm - 1033 nm). Among various strain value, the orthorhombic PdS_2 exhibits excellent piezoelectric effect (1.33 C/m^2) at 4% tensile deformation, which is 2-3 orders of magnitude higher than other deformation values. These excellent absorption and piezoelectric characteristics of the orthorhombic PdS_2 make it a compelling candidate for piezophototronic/piezoelectric devices and high sensitivity optical/strain sensors.

REFERENCES

[1] C.-H. Chang, *et al.*, "Orbital analysis of electronic structure and phonon dispersion in MoS2, MoSe2, WS2, and WSe2 monolayers under strain," *Physical Review B*, vol. 88, p. 195420, 2013.

[2] S. Deng, *et al.*, "Strain modulated electronic, mechanical, and optical properties of the monolayer PdS2, PdSe2, and PtSe2 for tunable devices," *ACS Applied Nano Materials*, vol. 1, pp. 1932-1939, 2018.

[3] L. J. Li and Y. Zhang, "Controlling the luminescence of monolayer MoS2 based on the piezoelectric effect," *Nano Research*, vol. 10, pp. 2527-2534,

Jul 2017.
[4] W. Z. Wu and Z. L. Wang, "Piezotronics and piezo-phototronics for adaptive electronics and optoelectronics," *Nature Reviews Materials*, vol. 1, Jul 2016.
[5] W. Z. Wu, *et al.*, "Piezoelectricity of single-atomic-layer MoS2 for energy conversion and piezotronics," *Nature*, vol. 514, pp. 470-+, Oct 2014.
[6] Y. K. Pang, *et al.*, "Tribotronic Enhanced Photoresponsivity of a MoS2 Phototransistor," *Advanced Science*, vol. 3, Jun 2016.
[7] C. Zhang, *et al.*, "Tribotronic Phototransistor for Enhanced Photodetection and Hybrid Energy Harvesting," *Advanced Functional Materials*, vol. 26, pp. 2554-2560, Apr 19 2016.
[8] W. Z. Wu, *et al.*, "Piezophototronic Effect in Single-Atomic-Layer MoS2 for Strain-Gated Flexible Optoelectronics," *Advanced Materials*, vol. 28, pp. 8463-8468, Oct 12 2016.
[9] C. Wu, *et al.*, "Enhanced Triboelectric Nanogenerators Based on MoS2 Monolayer Nanocomposites Acting as Electron-Acceptor Layers," *ACS Nano*, vol. 11, pp. 8356-8363, Aug 2017.
[10] Y. L. Zhou, *et al.*, "Theoretical study on two-dimensional MoS2 piezoelectric nanogenerators," *Nano Research*, vol. 9, pp. 800-807, Mar 2016.
[11] G. Y. Gao, *et al.*, "Tunable Tribotronic Dual-Gate Logic Devices Based on 2D MoS2 and Black Phosphorus," *Advanced Materials*, vol. 30, pp. 1-1, Mar 27 2018.
[12] F. Xue, *et al.*, "MoS2 Tribotronic Transistor for Smart Tactile Switch," *Advanced Functional Materials*, vol. 26, pp. 2104-2109, Apr 5 2016.
[13] K. D. Park, *et al.*, "Hybrid Tip-Enhanced Nanospectroscopy and Nanoimaging of Monolayer WSe2 with Local Strain Control," *Nano Letters*, vol. 16, pp. 2621-2627, Apr 2016.
[14] A. D. Oyedele, *et al.*, "PdSe2: Pentagonal Two-Dimensional Layers with High Air Stability for Electronics," *Journal of the American Chemical Society*, vol. 139, pp. 14090-14097, Oct 11 2017.
[15] M. G. Sensoy, *et al.*, "Strain effects on the behavior of isolated and paired sulfur vacancy defects in monolayer MoS2," *Physical Review B*, vol. 95, Jan 17 2017.
[16] S. Deng, *et al.*, "Stability of direct band gap under mechanical strains for monolayer MoS2, MoSe2, WS2 and WSe2," *Physica E-Low-Dimensional Systems & Nanostructures*, vol. 101, pp. 44-49, Jul 2018.
[17] S. Deng, *et al.*, "Strain Magnitude and Direction Effect on the Energy Band Structure of Hexagonal and Orthorhombic Monolayer MoS2," *IEEE Transactions on Nanotechnology*, vol. 17, pp. 419-423, May 2018.
[18] F. Gronvold and E. Rost, "The crystal structure of PdSe2 and PdS2," *Acta Crystallographica*, vol. 10, pp. 329-331, 1957.
[19] F. Gronvold, *et al.*, "On the sulfides, selenides and tellurides of platinum," *Acta Chemica Scandinavica*, vol. 14, pp. 1879-1893, 1960.
[20] L. Fu, *et al.*, "K-Lambda crossover transition in the conduction band of monolayer MoS2 under hydrostatic pressure," *Science Advances*, vol. 3, p. e1700162, Nov 2017.
[21] M. G. Sensoy, *et al.*, "Strain effects on the behavior of isolated and paired sulfur vacancy defects in monolayer MoS2," *Physical Review B*, vol. 95, p. 014106, Jan 17 2017.
[22] E. Scalise, *et al.*, "Strain-induced semiconductor to metal transition in the two-dimensional honeycomb structure of MoS2," *Nano Research*, vol. 5, pp. 43-48, Jan 2012.
[23] C. Soulard, *et al.*, "Experimental and theoretical investigation on the relative stability of the PdS2- and pyrite-type structures of PdSe2," *Inorganic Chemistry*, vol. 43, pp. 1943-1949, Mar 22 2004.
[24] M. Ghorbani-Asl, *et al.*, "A Single-Material Logical Junction Based on 2D Crystal PdS2," *Advanced Materials*, vol. 28, pp. 853-856, Feb 3 2016.
[25] W. Liu, *et al.*, "Density functional studies on edge-contacted single-layer MoS2 piezotronic transistors," *Applied Physics Letters*, vol. 107, Aug 24 2015.
[26] P. Johari and V. B. Shenoy, "Tuning the Electronic Properties of Semiconducting Transition Metal Dichalcogenides by Applying Mechanical Strains," *Acs Nano*, vol. 6, pp. 5449-5456, Jun 2012.
[27] W. Liu, *et al.*, "Theoretical study on the top- and enclosed-contacted single-layer MoS2 piezotronic transistors," *Applied Physics Letters*, vol. 108, May 2 2016.
[28] *Atomistix ToolKit (ATK), https://quantumwise.com/*.
[29] *Materials Project, https://materialsproject.com/*. .
[30] J. P. Perdew, *et al.*, "Generalized gradient approximation made simple," *Physical Review Letters*, vol. 77, pp. 3865-3868, Oct 28 1996.
[31] F. Tran and P. Blaha, "Accurate Band Gaps of Semiconductors and Insulators with a Semilocal Exchange-Correlation Potential," *Physical Review Letters*, vol. 102, p. 226401, Jun 5 2009.
[32] A. D. Becke and M. R. Roussel, "Exchange Holes in Inhomogeneous Systems - a Coordinate-Space Model," *Physical Review A*, vol. 39, pp. 3761-3767, Apr 15 1989.
[33] S. Grimme, "Semiempirical GGA-type density functional constructed with a long-range dispersion correction," *Journal of Computational Chemistry*, vol. 27, pp. 1787-1799, Nov 30 2006.
[34] J. Du, *et al.*, "Elastic, electronic and optical properties of the two-dimensional PtX2 (X = S, Se, and Te) monolayer," *Applied Surface Science*, vol. 435, pp. 476-482, Mar 30 2018.
[35] N. J. F., *Physical properties of crystals*: Oxford, 1985.
[36] *The Photographic Periodic Table of the Elements, https://periodictable.com/*. .
[37] D. Sadik and L. Brian, *Single Crystal Crowth of Semiconductors from Metallic Solutions*. Oxford: ELSEVIER, 2007.
[38] J. Chennupati and P. Stephen, *Zinc Oxide Bulk, Thin Films and Nanostructures Processing, Properties and Applications*. Oxford: ELSEVIER, 2006.
[39] B. Levl, *Semiconductor Materials*. New York: CRC Press, 1997.
[40] Y. Wang, *et al.*, "Not your familiar two dimensional transition metal disulfide: structural and electronic properties of the PdS2 monolayer," *Journal of Materials Chemistry C*, vol. 3, pp. 9603-9608, 2015.
[41] A. Hamidani, *et al.*, "Structural and electronic properties of the pseudo-binary compounds PdX2 (X = P, S and Se)," *Journal of Physics and Chemistry of Solids*, vol. 71, pp. 42-46, Jan 2010.
[42] R. D. Kingsmith and D. Vanderbilt, "Theory of Polarization of Crystalline Solids," *Physical Review B*, vol. 47, pp. 1651-1654, Jan 15 1993.
[43] F. Bernardini, *et al.*, "Spontaneous polarization and piezoelectric constants of III-V nitrides," *Physical Review B*, vol. 56, pp. 10024-10027, Oct 15 1997.

Shuo Deng is currently a visiting student with the College of Engineering, Swansea University, Swansea, U.K. His research interests include first principles study.

Menglun Tao is an associate professor in school of logistics engineering, Wuhan University of Technology. His research interests include mechanical engineering.

Jie Mei is an associate professor in school of logistics engineering, Wuhan University of Technology. His research interests include mechanical energy harvesting devices.

Min Li is a professor in school of science, Wuhan University of Technology. Her research interests include applied physics.

Yan Zhang (SM'18) is a professor with the School of Physics, School of Physical Electronics, University of Electronic Science and Technology of China, Chengdu, China. His research interests include NEMS, piezotronics, piezo-phototronics, semiconductor, and nanotechnology.

Lijie Li (SM'10) is a professor with the College of Engineering, Swansea University, Swansea, U.K. His research interests include MEMS, NEMS, sensors and actuators, and piezotronics.